Research Article | Vol. 9, No. 9 | 1 Sep 2018 | BIOMEDICAL OPTICS EXPRESS 4401
Biomedical Optics EXPRESS

Ex vivo classification of spinal cord tumors using autofluorescence spectroscopy and immunohistochemical indexes

MINGYU ZHU,[1] FANG CHEN,[1] JIA LIU,[1] GUIHUAI WANG,[2] AND HONGEN LIAO[1*]

[1]*Department of Biomedical Engineering, School of Medicine, Tsinghua University, Beijing 100084, China*
[2]*Department of Neurosurgery, Beijing Tsinghua Changgung Hospital, Beijing 102218, China*
**liao@tsinghua.edu.cn*

Abstract: Spinal cord tumors are complicated and infrequent, which poses a major challenge to surgeons during neurosurgery. Currently, the intraoperative identification of the tissues' pathological properties is usually difficult for surgeons. This issue influences the decision-making in treatment planning. Traditional pathological diagnoses can facilitate judging the tissues' properties, but the diagnosis process is complex and time-consuming. In this study, we evaluated the potential of autofluorescence spectroscopy for the fast pathological diagnosis of specific spinal cord tumors. The spectral properties of six types of spinal cord tumors were acquired *ex vivo*. Several peak intensity ratios were calculated for classification and then associated with the pathological immunohistochemical indexes. Our results revealed the spectral properties of three types of intramedullary tumors different from those of the other three types of extramedullary tumors. Furthermore, some peak intensity ratios revealed a high correlation with the immunohistochemical index of glial fibrillary acidic protein (GFAP). Thus, we believe that autofluorescence spectroscopy has the potential to provide real-time pathological information of spinal cord tumors and help surgeons validate tumor types and perform precise tumor resection.

OCIS codes: (170.6280) Spectroscopy, fluorescence and luminescence; (170.6935) Tissue characterization; (170.1610) Clinical applications; (170.6510) Spectroscopy, tissue diagnostics; (170.4730) Optical pathology.

References and links

1. C. Espina, M. Porta, J. Schüz, I. H. Aguado, R. V. Percival, C. Dora, T. Slevin, J. R. Guzman, T. Meredith, P. J. Landrigan, and M. Neira, "Environmental and occupational interventions for primary prevention of cancer: a cross-sectorial policy framework," Environ. Health Perspect. **121**(4), 420–426 (2013).
2. Y. Li, R. Rey-Dios, D. W. Roberts, P. A. Valdés, and A. A. Cohen-Gadol, "Intraoperative fluorescence-guided resection of high-grade gliomas: a comparison of the present techniques and evolution of future strategies," World Neurosurg. **82**(1-2), 175–185 (2014).
3. C. Chi, Y. Du, J. Ye, D. Kou, J. Qiu, J. Wang, J. Tian, and X. Chen, "Intraoperative imaging-guided cancer surgery: from current fluorescence molecular imaging methods to future multi-modality imaging technology," Theranostics **4**(11), 1072–1084 (2014).
4. P. A. Valdés, D. W. Roberts, F.-K. Lu, and A. Golby, "Optical technologies for intraoperative neurosurgical guidance," Neurosurg. Focus **40**(3), E8 (2016).
5. T. Ando, E. Kobayashi, H. Liao, T. Maruyama, Y. Muragaki, H. Iseki, O. Kubo, and I. Sakuma, "Precise comparison of protoporphyrin IX fluorescence spectra with pathological results for brain tumor tissue identification," Brain Tumor Pathol. **28**(1), 43–51 (2011).
6. H. Liao, M. Noguchi, T. Maruyama, Y. Muragaki, E. Kobayashi, H. Iseki, and I. Sakuma, "An integrated diagnosis and therapeutic system using intra-operative 5-aminolevulinic-acid-induced fluorescence guided robotic laser ablation for precision neurosurgery," Med. Image Anal. **16**(3), 754–766 (2012).
7. H. Liao, K. Fujiwara, T. Ando, T. Maruyama, E. Kobayashi, Y. Muragaki, H. Iseki, and I. Sakuma, "Automatic laser scanning ablation system for high-precision treatment of brain tumors," Lasers Med. Sci. **28**(3), 891–900 (2013).
8. W. Stummer, U. Pichlmeier, T. Meinel, O. D. Wiestler, F. Zanella, and H.-J. Reulen, "Fluorescence-guided surgery with 5-aminolevulinic acid for resection of malignant glioma: a randomised controlled multicentre phase III trial," Lancet Oncol. **7**(5), 392–401 (2006).

#338394 https://doi.org/10.1364/BOE.9.004401
Journal © 2018 Received 10 Jul 2018; revised 5 Aug 2018; accepted 5 Aug 2018; published 21 Aug 2018

Biomedical Optics EXPRESS

9. S. Shimizu, S. Utsuki, K. Sato, H. Oka, K. Fujii, and K. Mii, "Photodynamic diagnosis in surgery for spinal ependymoma. case illustration," J. Neurosurg. Spine **5**(4), 380 (2006).
10. C. Ewelt, W. Stummer, B. Klink, J. Felsberg, H. J. Steiger, and M. Sabel, "Cordectomy as final treatment option for diffuse intramedullary malignant glioma using 5-ALA fluorescence-guided resection," Clin. Neurol. Neurosurg. **112**(4), 357–361 (2010).
11. M. Rapp, M. Klingenhöfer, J. Felsberg, H. J. Steiger, W. Stummer, and M. Sabel, "Fluorescence-guided resection of spinal metastases of malignant glioma: report of 2 cases," J. Neurol. Surg. A Cent. Eur. Neurosurg. **73**(2), 103–105 (2012).
12. T. Inoue, T. Endo, K. Nagamatsu, M. Watanabe, and T. Tominaga, "5-aminolevulinic acid fluorescence-guided resection of intramedullary ependymoma: report of 9 cases," Neurosurgery **72**(2), ons159–ons168, discussion ons168 (2013).
13. M. Millesi, B. Kiesel, A. Woehrer, J. A. Hainfellner, K. Novak, M. Martínez-Moreno, S. Wolfsberger, E. Knosp, and G. Widhalm, "Analysis of 5-aminolevulinic acid-induced fluorescence in 55 different spinal tumors," Neurosurg. Focus **36**(2), E11 (2014).
14. K. Vishwanath and N. Ramanujam, "Fluorescence spectroscopy in vivo," in *Encyclopedia of Analytical Chemistry,* R. A. Meyers, ed. (John Wiley & Sons Ltd. 2006).
15. A. C. Croce and G. Bottiroli, "Autofluorescence spectroscopy and imaging: a tool for biomedical research and diagnosis," Eur. J. Histochem. **58**(4), 2461 (2014).
16. W.-C. Lin, S. A. Toms, M. Motamedi, E. D. Jansen, and A. Mahadevan-Jansen, "Brain tumor demarcation using optical spectroscopy; an in vitro study," J. Biomed. Opt. **5**(2), 214–220 (2000).
17. A. Saraswathy, R. S. Jayasree, K. V. Baiju, A. K. Gupta, and V. P. Pillai, "Optimum wavelength for the differentiation of brain tumor tissue using autofluorescence spectroscopy," Photomed. Laser Surg. **27**(3), 425–433 (2009).
18. A. C. Croce, U. De Simone, I. Freitas, E. Boncompagni, D. Neri, U. Cillo, and G. Bottiroli, "Human liver autofluorescence: an intrinsic tissue parameter discriminating normal and diseased conditions," Lasers Surg. Med. **42**(5), 371–378 (2010).
19. W. Zheng, W. Lau, C. Cheng, K. C. Soo, and M. Olivo, "Optimal excitation-emission wavelengths for autofluorescence diagnosis of bladder tumors," Int. J. Cancer **104**(4), 477–481 (2003).
20. B.-H. Li and S.-S. Xie, "Autofluorescence excitation-emission matrices for diagnosis of colonic cancer," World J. Gastroenterol. **11**(25), 3931–3934 (2005).
21. L. F. Eng, R. S. Ghirnikar, and Y. L. Lee, "Glial fibrillary acidic protein: GFAP-thirty-one years (1969-2000)," Neurochem. Res. **25**(9/10), 1439–1451 (2000).
22. A. C. Croce, S. Fiorani, D. Locatelli, R. Nano, M. Ceroni, F. Tancioni, E. Giombelli, E. Benericetti, and G. Bottiroli, "Diagnostic potential of autofluorescence for an assisted intraoperative delineation of glioblastoma resection margins," Photochem. Photobiol. **77**(3), 309–318 (2003).
23. Y. G. Chung, J. A. Schwartz, C. M. Gardner, R. E. Sawaya, and S. L. Jacques, "Diagnostic potential of laser-induced autofluorescence emission in brain tissue," J. Korean Med. Sci. **12**(2), 135–142 (1997).
24. M. Stoeckli, P. Chaurand, D. E. Hallahan, and R. M. Caprioli, "Imaging mass spectrometry: a new technology for the analysis of protein expression in mammalian tissues," Nat. Med. **7**(4), 493–496 (2001).
25. L. S. Eberlin, I. Norton, D. Orringer, I. F. Dunn, X. Liu, J. L. Ide, A. K. Jarmusch, K. L. Ligon, F. A. Jolesz, A. J. Golby, S. Santagata, N. Y. Agar, and R. G. Cooks, "Ambient mass spectrometry for the intraoperative molecular diagnosis of human brain tumors," Proc. Natl. Acad. Sci. U.S.A. **110**(5), 1611–1616 (2013).
26. J. Q. Nguyen, Z. Gowani, M. O'Connor, I. Pence, T. Q. Nguyen, G. Holt, and A. Mahadevan-Jansen, "Near-infrared autofluorescence spectroscopy of in vivo soft tissue sarcomas," Opt. Lett. **40**(23), 5498–5501 (2015).
27. T. Svensson, S. Andersson-Engels, M. Einarsdóttír, and K. Svanberg, "In vivo optical characterization of human prostate tissue using near-infrared time-resolved spectroscopy," J. Biomed. Opt. **12**(1), 014022 (2007).
28. T. Zhou, T. Ando, K. Nakagawa, H. Liao, E. Kobayashi, and I. Sakuma, "Localizing fluorophore (centroid) inside a scattering medium by depth perturbation," J. Biomed. Opt. **20**(1), 017003 (2015).
29. H. Liao, T. Inomata, I. Sakuma, and T. Dohi, "3-D augmented reality for MRI-guided surgery using integral videography autostereoscopic image overlay," IEEE Trans. Biomed. Eng. **57**(6), 1476–1486 (2010).
30. Y. Fan, Y. Sun, W. Chang, X. Zhang, J. Tang, L. Zhang, and H. Liao, "Bioluminescence imaging and two-photon microscopy guided laser ablation of GBM decreases tumor burden in a mouse model," Theranostics **8**(15), 4072–4085 (2018).
31. H. Liao, "Integrated diagnostic and therapeutic techniques: Toward an intelligent medical system," Comput. Med. Imaging Graph. **38**(5), 421–422 (2014).

1. Introduction

Tumor diseases are well-recognized as a severe threat to the human health. It is estimated that tumor diseases may result in almost 7.6 million deaths annually all over the world in 2013 [1]. Among all tumor diseases known, the nervous system tumor is one of the most difficult tumors to be treated, such as brain tumors and spinal cord tumors. For most nervous system tumors, surgical resection is the most effective treatment method. However, currently, intraoperative identification of tissues' pathological information is difficult for surgeons. In

Biomedical Optics EXPRESS

neurosurgery, this pathological information is critical for surgeons because different types of diseases may require different treatment plans [2]. If surgeons are unsure about the tumor type, it is possible to develop an inadequate treatment plan and influence the treatment effect. Therefore, accurate pathological information of the tissues is crucial for neurosurgery.

Conventional medical imaging techniques, such as computed tomography (CT) and magnetic resonance imaging (MRI), provide preoperative information with high spatial resolutions for surgeons to develop a treatment plan; however, these two imaging methods do not provide real-time information. Intraoperative MRI (iMRI) and ultrasound imaging (US) possess the potential for real-time diagnosis, whereas iMRI is expensive and has a high demand for the operating room, and the use of US is limited because of the low quality images produced [3]. Furthermore, these abovementioned imaging techniques rarely provide accurate pathological information. Currently, frozen pathological biopsy is widely preferred for intraoperative tissue identification; however, this technique is time-consuming and complex. Therefore, it is deemed necessary to develop a more convenient method that can provide accurate pathological diagnostic information in a short time.

Optical biopsy is a promising method for fast intraoperative diagnosis. This method applies the phenomenon of interaction between light and the examined tissues, such as scattering and reflection, to obtain pathological information. The common optical diagnostic methods include Raman spectroscopy, optical coherence tomography, fluorescence imaging and spectroscopy [4]. In this study, we focused on fluorescence imaging and spectroscopy in consideration of its convenience for medical application [5–7]. Fluorescence may be sourced from extrinsic or intrinsic agents, and the corresponding imaging and spectroscopic methods can provide real-time diagnostic information. Fluorescence imaging by using extrinsic fluorescent agents such as 5-aminolevulinic acid (5-ALA)-induced protoporphyrin IX is widely studied and can provide intraoperative imaging of tumors [8]. Shimizu et al. [9] reported the application of photodynamic diagnosis in surgery for spinal ependymoma. Sabel et al. [10,11] used 5-ALA fluorescence-guided resection to treat intramedullary malignant glioma. Inoue et al. [12] applied 5-ALA fluorescence to the resection of intramedullary ependymoma. Millesi et al. [13] also investigated 5-ALA-induced fluorescence characteristics of spinal tumors. All these researches have illustrated that 5-ALA-induced fluorescence is able to help surgeons discriminate tumors better and thus improve the operation safety. However, the mechanism of 5-ALA-induced fluorescence remains unclear, and for some types of spinal tumors, 5-ALA-induced fluorescence cannot be observed. Besides, 5-ALA-induced fluorescence is hard to be used for the discrimination of different types of spinal tumors.

Autofluorescence arises from some intrinsic fluorescent agents when excited by specific wavelengths in biological tissues such as porphyrin, collagen, and flavin [14,15]. Autofluorescence spectroscopy is a kind of label-free diagnosis that may provide more information about tumors' pathological properties for fast classification, and some relevant researches have been carried out. Lin et al. [16] used autofluorescence combined with diffuse reflectance spectroscopy to measure the different parameters between the normal and tumorous brain tissues, and the corresponding algorithms based on these parameters were highly sensitive and specific. Saraswathy et al. [17] also used autofluorescence spectroscopy to test the optimum wavelength for the differentiation of brain tumors and thereby suggested an optimal excitation wavelength of 470 nm. Other researchers also applied autofluorescence spectroscopy to the liver, bladder, and colon tissues [18–20] and concluded that autofluorescence spectroscopy may be a fast and accurate method for intraoperative diagnosis.

Spinal cord tumors have a low incidence and are challenging to surgeons owing to the important functions of the normal spinal cord. However, few researchers have studied the optical properties of spinal cord tumors. In this study, we developed an autofluorescence spectral measurement system to acquire the spectral properties of different types of spinal

Biomedical Optics EXPRESS

cord tumors *ex vivo* and further analyzed the correlation between autofluorescence spectroscopy and pathological diagnosis of spinal cord tumors. The main objectives of our study were to evaluate whether autofluorescence spectroscopy could be used for the classification of different spinal cord tumors as well as to further correlate the spectroscopy with pathological immunohistochemical indexes for fast intraoperative diagnosis.

2. Materials and methods

2.1 Autofluorescence spectral measurement system

Our spectral measurement system was mainly composed of a monochromatic light source, a sample chamber, an emission monochromator and a detector (Fig. 1). The monochromatic light source consisted of a 150-W xenon light source and an excitation monochromator (Omni-3028i; Zolix Instrument, Beijing, China) in consideration of the adjustable excitation wavelengths. Monochromatic light from the excitation monochromator was projected onto the sample placed on a holder in the sample chamber (SAC-FS; Zolix Instrument). Emission light was projected to the emission monochromator and then captured by the electron-multiplying charge-coupled device (EMCCD) camera (iXon Ultra 888; Andor Technology, Oxford, UK). The two monochromators and the EMCCD camera were controlled by a personal computer. The slit sizes of the excitation and emission monochromator were set to 1.2 and 0.8 mm, respectively. The available scanning range of our system was 200–1000 nm and the bandwidth was 15 nm.

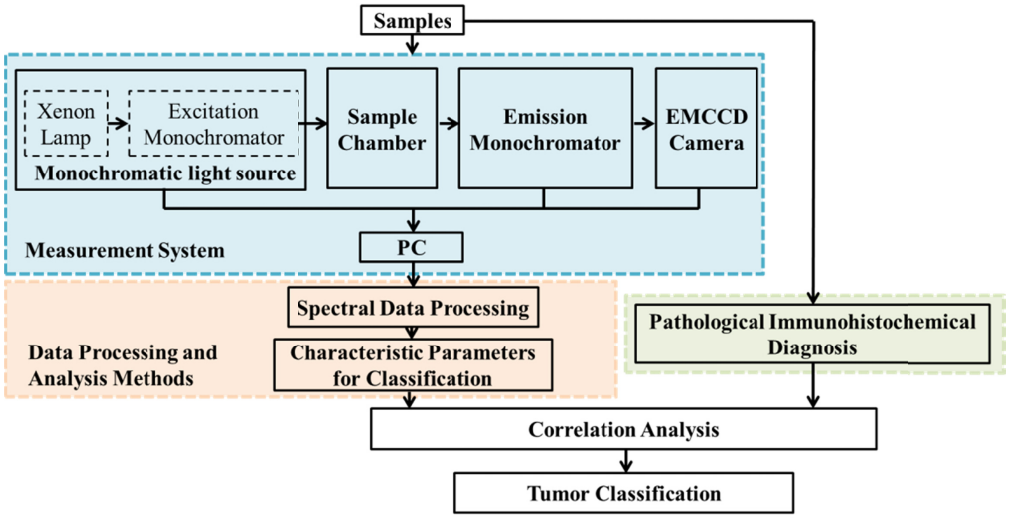

Fig. 1. Configuration of the measurement system and analysis methods.

2.2 Spinal cord tumor specimens

The spinal cord tumor tissues were obtained from 41 Chinese patients during tumor resection performed at the Beijing Tsinghua Changgung Hospital between July and November 2017. The basic information about the acquired tumor tissues is listed in Table 1. A total of six spinal cord tumor types were involved. Our research was approved by the Ethics Committee of Beijing Tsinghua Changgung Hospital, and all patients provided their signed informed consent. After resection, the tissues were drenched in saline to remove the residual blood and then subjected to spectral measurement within 5 min. The tissues were cut to maintain a consistent thickness of 4-5 mm. In the process of spectral measurement, saline was sprayed onto the tissues several times to avoid drying. After spectral measurement, the tissues were dispatched for pathological examination to obtain pathological and immunohistochemical diagnosis for further study.

Biomedical Optics EXPRESS

Table 1. Information about spinal cord tumor tissues

Tumor Type	Number of Patients	Age Range (y)	Sex Ratio (Male:Female)	Measurement Points
Schwannoma	11	18-70	7:4	68
Ependymoma	10	28-61	5:5	54
Meningeoma	7	43-72	3:4	43
CNSET	3	17-30	3:0	17
GBM	4	9-32	2:2	26
Lipomyoma	6	24-49	4:2	39

(CNSET = central nervous system embryonal tumor, GBM = glioblastoma multiforme)

2.3 Spectral measurement methods

In order to achieve the signal with the best signal to noise ratio, once the sample was placed on the holder, a stable spectral scanning was performed. Excitation light was projected onto the sample at an incident angle of 60°, and the emission light was collected at 45° with respect to the sample holder so that the interference of the backscattered excitation light could be reduced. The excitation irradiance was 30 mW/cm^2 at the exit slit of the excitation monochromator. The diameter of the excitation light spot was kept as 0.2 cm. The integration time of the EMCCD camera was set to 0.5 s; the EM gain was set to 4 times; and the cryogenic temperature of the EMCCD was set to −60°C. We selected 400 nm for the excitation wavelength and set 610–639 nm for the spectral scanning range, which corresponded with the emission peak of porphyrins. The position of the holder was adjusted to achieve the maximum emission peak, and the position was fixed for the sample within the spectral measurement process. The procedure was conducted only at the beginning of each measurement for the initial mechanical adjustment of the sample within the sample chamber.

For each sample, an excitation-emission matrix (EEM) was acquired. The excitation wavelength varied from 280 nm to 450 nm (ultraviolet-visible range; UV-VIS) at 10-nm increments. At each excitation wavelength, the autofluorescence emission spectrum was recorded from a range starting at 40-nm above the excitation wavelength and up to twice the excitation wavelength (no more than 750 nm). It took about 15 min to acquire an EEM. To increase the number of spectral data and to improve the accuracy of data analysis, we measured different points for each sample. As the size of each sample was different (Fig. 2), at least five different points were measured. The total measurement points are listed in Table 1. The standard deviation of spectral measurements for each sample was 1.21. Considering that each acquisition of an EEM was time-consuming, EEM was acquired at only one measurement point. At the remaining measurement points, only five featured spectra at the excitation wavelength of 280, 330, 350, 400, and 450 nm were acquired. At the end of each EEM scan, the autofluorescence spectrum at 330-nm excitation wavelength was measured again to ascertain whether photobleaching occurred, and the background noise was recorded for data analysis.

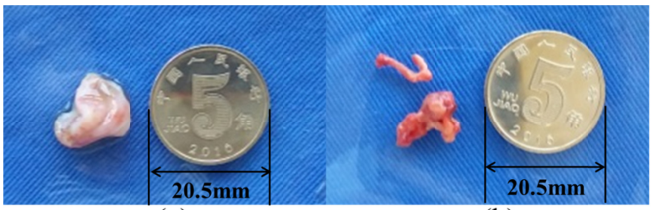

Fig. 2. (a,b) Two spinal cord tumor samples with different sizes. At least five measurement points were used to acquire an effective spectral data.

Biomedical Optics EXPRESS

2.4 Spectral data processing and correlation analysis

After spectral scanning, all data were processed before forming EEMs and further analysis. Background noise subtraction was first performed, and all spectral data were normalized to the respective wavelength position of the maximum intensity excited by 400-nm wavelength (corresponding to the emission of porphyrins) in order to enable the comparison between different tumor samples. EEMs were formed with the normalized data by using the Origin 10.0 (OriginLab, USA). In order to classify the different types of spinal cord tumors, we created several groups of peak intensity ratios. We then evaluated the differences of these ratios among different types of tumors and evaluated their relationship with immunohistochemistry through correlation analysis. Data processing was completed by using Matlab 2016 (MathWorks, USA), and data analysis was performed by using SPSS 23.0 (IBM, USA).

3. Results

A total of 41 patients with different spinal cord tumors were enrolled in this study. The prototype of our measurement system and the measurement setting are shown in Fig. 3.

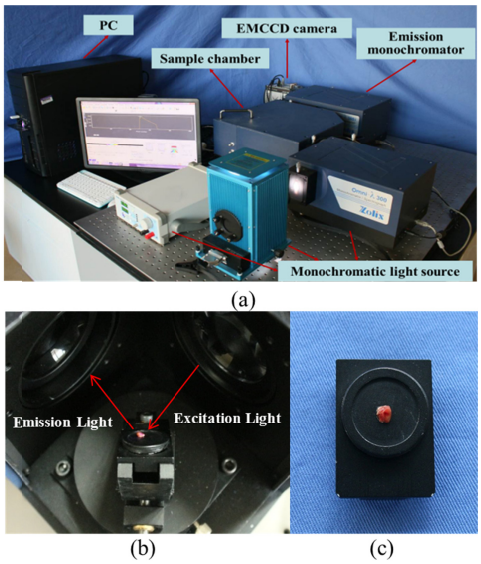

Fig. 3. (a) Prototype of the proposed measurement system, (b) measurement setting in the sample chamber, and (c) tumor specimen on the holder.

No obvious photobleaching occurred during the whole measurement process. Figure 4 shows the EEMs and the corresponding pathological section images of six different types of spinal cord tumor samples. All these EEMs contained three characteristic fluorescence peaks, i) centered at 470 nm when excited by a 320–370 nm wavelength, ii) at 550 nm when excited by a 350–380 nm wavelength, and iii) at 620 nm when excited by a 380–410 nm wavelength. Furthermore, the EEMs of the schwannoma, meningeoma, and lipomyoma showed a particular fluorescence peak centered at 394 nm when excited by a 310–340 nm wavelength, and the EEMs of the ependymoma, CNS embryonal tumor, and glioblastoma multiforme showed a particular fluorescence peak centered at 520 nm when excited by a 440–450 nm wavelength. Figure 5 shows the normalized average spectral curves of six different spinal cord tumors at five excitation wavelengths. It can be seen from the figure that the normalized spectral curves of six types of tumors appears to be divided into two classes at 330 and 450 nm excitation.

Biomedical Optics EXPRESS

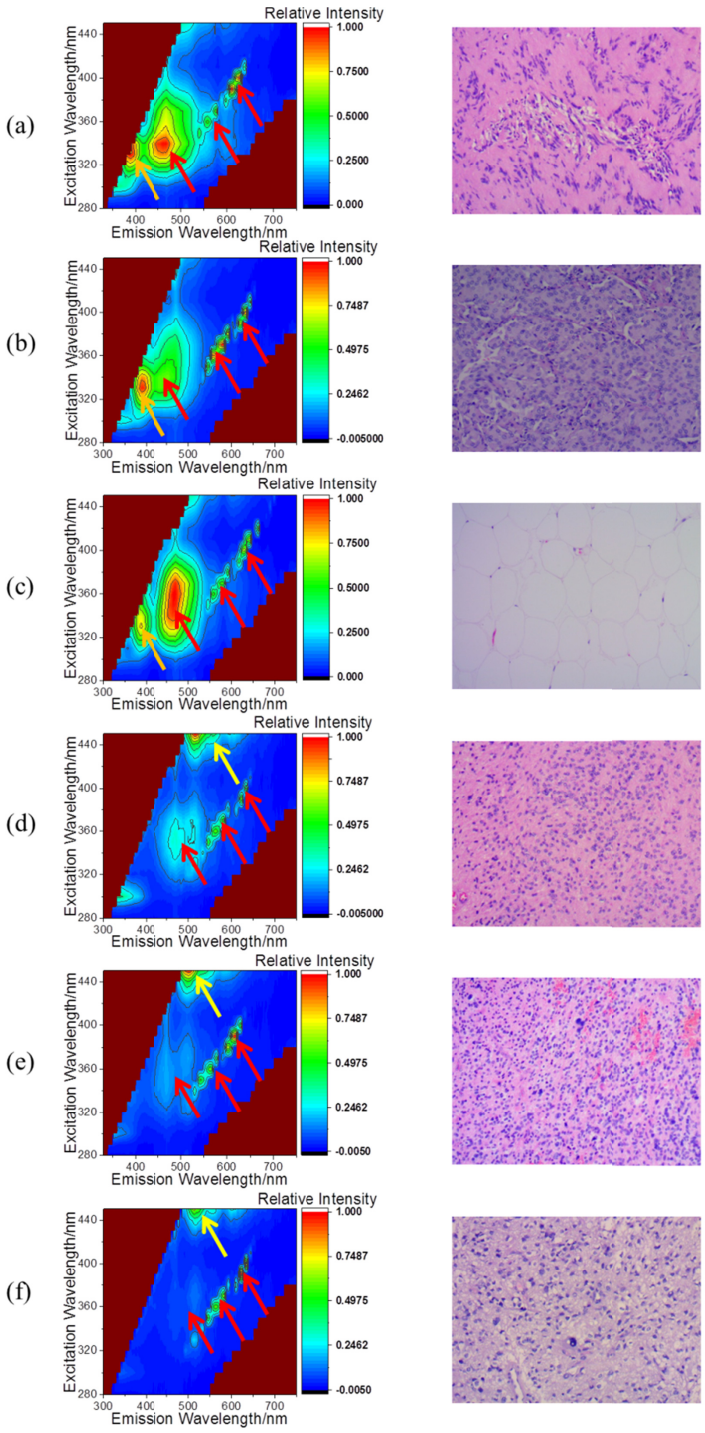

Fig. 4. EEMs (left) and the corresponding pathological images (right) of six types of spinal cord tumors: (a) Schwannoma, (b) Meningeoma, (c) Lipomyoma, (d) Ependymoma, (e) CNS embryonal tumor, and (f) Glioblastoma multiforme. Red arrows refer to the three common peaks, while the orange and yellow arrows refer to the specific peaks of two groups of tumors.

Biomedical Optics EXPRESS

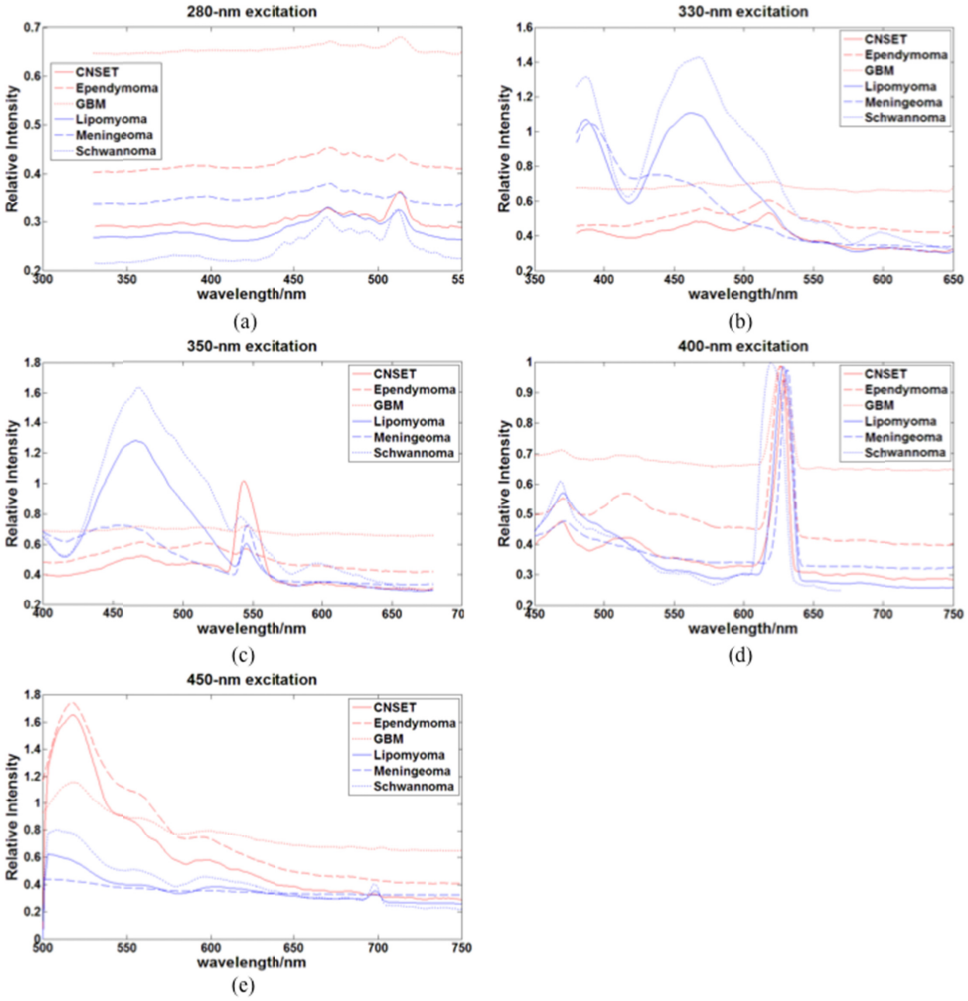

Fig. 5. Normalized average spectral curves: (a) 280-nm excitation wavelength, (b) 330-nm excitation wavelength, (c) 350-nm excitation wavelength, (d) 400-nm excitation wavelength and (e) 450-nm excitation wavelength. Red and blue curves may possibly indicate that six types of tumors can be classified into two classes.

In order to validate whether the above spectral difference at the excitation wavelengths of 330 nm and 450 nm could be validated for all samples for tumor classification, we further compared the distribution of several normalized peak intensity ratios. A total of five normalized peak intensity ratios including $I_{280\text{-}512}/I_{400\text{-}633}$ (R_1, $I_{280\text{-}512}$ means the spectral intensity at the emission wavelength of 512 nm excited by 280-nm wavelength, and the remaining can be done in the same manner), $I_{330\text{-}394}/I_{400\text{-}633}$ (R_2), $I_{350\text{-}464}/I_{400\text{-}633}$ (R_3), $I_{350\text{-}546}/I_{400\text{-}633}$ (R_4), and $I_{450\text{-}520}/I_{400\text{-}633}$ (R_5), were observed and compared. The values of R_2 and R_5 showed a clustering but no significant distribution, while the other three values did not show any clustering, as shown in Fig. 6(a)–(e). In order to classify tumors better, we further calculated the other relative peak intensity ratios by pairwise division of $I_{280\text{-}512}$, $I_{330\text{-}394}$, $I_{350\text{-}464}$, $I_{350\text{-}546}$, and $I_{450\text{-}520}$. We found that the values of $I_{330\text{-}394}/I_{450\text{-}520}$ (R_6), $I_{350\text{-}464}/I_{450\text{-}520}$ (R_7), and $I_{350\text{-}546}/I_{450\text{-}520}$ (R_8) emerged as an obvious clustering distribution among different types of tumors, as shown in Fig. 6(f)–(h). We used an unpaired student's t-test and found that the values of R_6, R_7, and R_8 in the lipomyoma, meningioma, and schwannoma were significantly larger than those in CNSET, ependymoma, and GBM ($p<0.01$).

Biomedical Optics EXPRESS

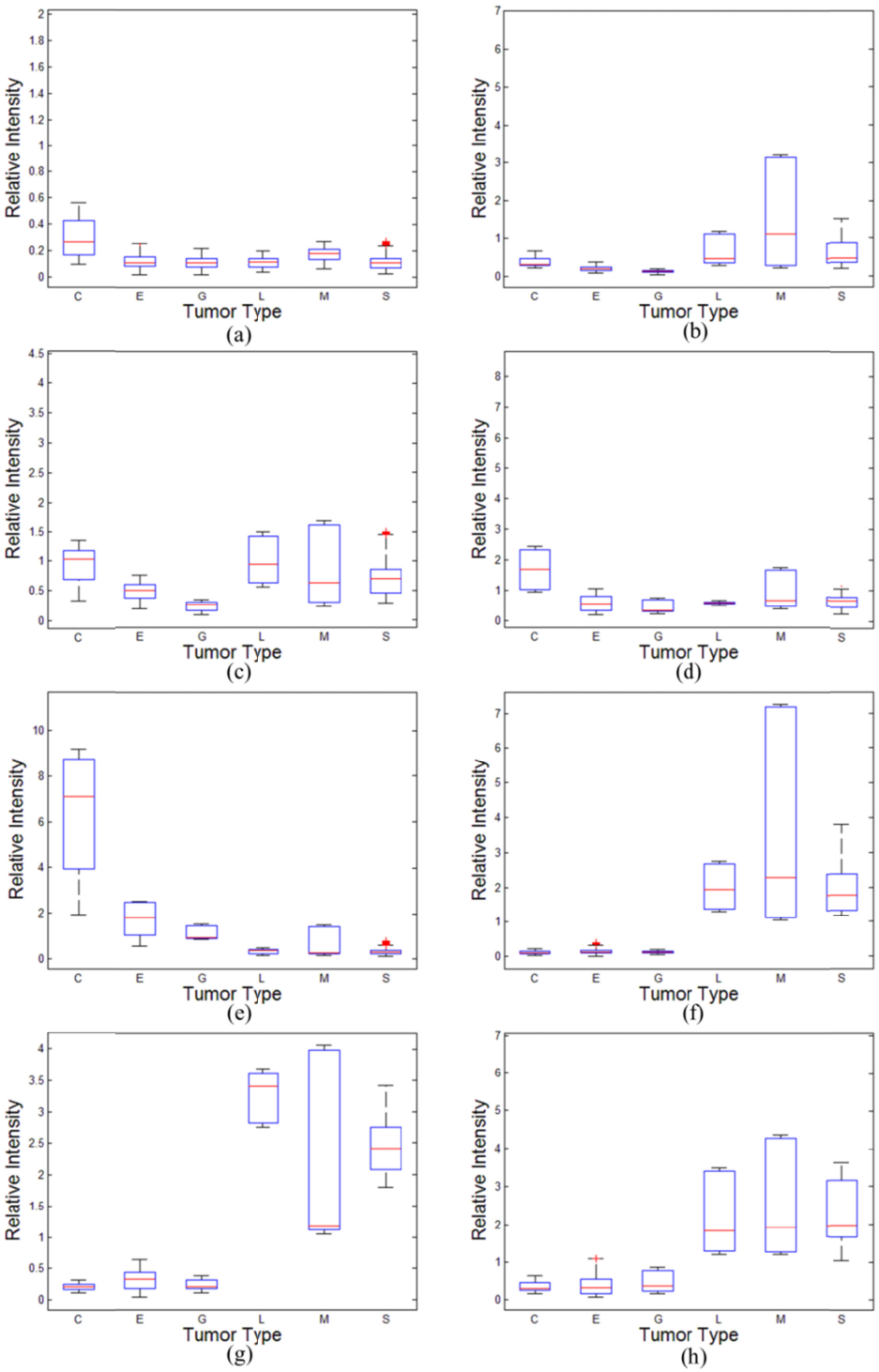

Fig. 6. Distribution of the values of some peak intensity ratios: (a) R_1, (b) R_2, (c) R_3, (d) R_4, (e) R_5, (f) R_6, (g) R_7, and (h) R_8. (C = CNSET, E = Ependymoma, G = GBM, L = Lipomyoma, M = Meningioma, S = Schwannoma).

Biomedical Optics EXPRESS

To further analyze the correlation between the clustering distribution of peak intensity ratios and the spinal cord tumor type, the immunohistochemical results were considered. Several immunohistochemical indexes, such as S-100, GFAP, and Epithelial Membrane Antigen (EMA), if present, were acquired. Correlation analysis was applied to analyze the relationship between the peak intensity ratios and immunohistochemical indexes (Table 2). The results of correlation analysis indicated that the relative peak intensity ratios R_6, R_7, and R_8 shared a high and significant correlation with the GFAP expression. The tumors with negative GFAP are likely to achieve high R_6, R_7, and R_8 values (>1.0), in contrast, the tumors with positive GFAP are likely to achieve low R_6, R_7, and R_8 values (<1.0). GFAP exists in mature astrocytes of the human central nervous system; it is a type of intermediate filament and plays an important role in cell regulation [21]. GFAP also exists as a type of biomarker that indicates some kinds of tumors' malignancy and prognosis. The correlation between the GFAP expression and the values of relative peak intensity ratios possibly indicates that the GFAP expression may be correlated with the content of some intrinsic fluorescent agents in the tumorous tissues.

Furthermore, we also found that all ependymoma, CNS embryonal tumor and glioblastoma multiforme in our study were intramedullary. On the contrary, all lipomyoma, meningioma and schwannoma were extramedullary. This observation corresponded with the common performance of spinal cord tumors. In other words, most intramedullary tumors are likely to perform positive GFAP and possess low R_6, R_7, and R_8 values (<1.0), while most extramedullary tumors are likely to perform negative GFAP and possess high R_6, R_7, and R_8 values (>1.0).

Table 2. Pearson's R Coefficient Between Peak Intensity Ratios (PIR) and Immunohistochemical Indexes (IMI)

PIR \ IMI	GFAP	EMA	S-100
R_6	**–0.742 (P < 0.001)**	–0.359 (P = 0.019)	–0.327 (P = 0.035)
R_7	**–0.903 (P < 0.001)**	–0.643 (P = 0.001)	–0.092 (P = 0.562)
R_8	**–0.745 (P < 0.001)**	–0.486 (P = 0.001)	–0.158 (P = 0.319)

(Positive IMI denotes 1; Negative IMI denotes 0)

4. Discussion

This study involved a total of 41 patients with six different types of spinal cord tumors. We conducted autofluorescence spectral measurements to evaluate the diagnostic potential of autofluorescence spectroscopy in these patients. To the best of our knowledge, this is the first application of autofluorescence spectroscopy to spinal cord tumors, mainly due to the relative low incidence of spinal cord tumors. In order to differentiate the six types of spinal cord tumors, several peak intensity ratios were calculated. The different peak intensity ratios of spinal cord tumors possibly indicated the different contents of endogenous fluorophores. We found that the values of R_6, R_7, and R_8 were larger in extramedullary tumors like lipomyoma, meningioma, and schwannoma than in intramedullary tumors like CNSET, ependymoma, and GBM. Furthermore, we analyzed the correlation between the autofluorescence properties and immunohistochemical indexes and found that the values of R_6, R_7, and R_8 were inversely proportional to the GFAP index. In other words, the GFAP expression may influence the relative intensity of autofluorescence spectrum, possibly indicating that GFAP is related to the amount of endogenous fluorophores in spinal cord tumors. This finding is believed to be extremely useful for clinical application. In neurosurgery, surgeons usually require different treatment plans for intramedullary or extramedullary tumors. Our proposed technique can provide fast pathological information of tumors, which will assist surgeons in judging the tumor type and therefore in planning a corresponding treatment plan to achieve better clinical outcomes.

Biomedical Optics EXPRESS

From the measurement data, we now know that the major UV-VIS endogenous fluorophores in spinal cord tumors are mainly coincident with those in other human tumor tissues [16–20]. The emergence of the three common fluorescence peaks may be attributed to the emission of NAD(P)H, lipopigments, and porphyrins, respectively [14,22,23]. The particular fluorescence peak centered at 520 nm may arise due to the emission of flavin adenine dinucleotide and flavins [14,15], while the fluorochrome responsible for the fluorescence peak centered at 394 nm remained uncertain. The fluorochromes close to this excitation-emission band include structural proteins like collagen and elastin as well as vitamin B6 compounds like pyridoxine and pyridoxal 5′-phosphate [14]. Generally, Collagen does not exist in the brain tissues [22]. However, Saraswathy et al. [17] indicated that collagen might be responsible for one of the emission bands at 320-nm excitation in the brain tumor autofluorescence. To clarify which fluorochromes are responsible for the emission of spinal cord tumors and to further explain the correlation between different fluorochromes and GFAP expression, we will investigate the spectra and composition of more different spinal cord tumors by using additional other methods like mass spectrometry [24,25].

Spinal cord tumors occur in several types, and each type may have a unique autofluorescence spectral property. In fact, even the same tumor type may possess different optical properties when their growth environment is different. Therefore, it is deemed essential to validate the generalizability of our observations. In the future, we plan to analyze more kinds of spinal cord tumors for more precise tumor analysis, validate our conclusion that intramedullary and extramedullary tumors have different autofluorescence properties, and further explain the correlation between immunohistochemical indexes and autofluorescence spectroscopy. Our present results indicate that different types of intramedullary (or extramedullary) tumor demonstrate similar EEM and that it is difficult to distinguish within the intramedullary (or extramedullary) tumor group based on the currently available methods. Therefore, more excitation wavelengths like near-infrared (NIR) band and the corresponding techniques such as time-resolved spectroscopy and fluorophore localizing are believed to provide detailed information about tissues' properties [26–28], and thereby further improve the diagnostic efficiencies for precision medicine [29–31].

The grading of tumors is important for surgeons to decide the appropriate treatment plan. Currently, the grading of tumors is acquired by pathological diagnosis. Mitosis, cellular pleomorphism and cell morphology are the common methods used to grade a tumor. Some immunohistochemical indexes such as S-100 and Ki-67 may assist in judging the grading of a tumor. In this study, we found that autofluorescence spectroscopy of spinal cord tumors was related to the immunohistochemical indexes that were relevant with tumor grading. Thus, we believe that our method has the potential to assist tumor grading. In the future, we plan to expand the tumor samples for analyses with different grading in order to investigate the quantitative relationship between autofluorescence spectroscopy and tumor grading so as to develop new processing methods for faster grading of spinal cord tumors.

All spectral measurement experiments in this study were performed *ex vivo*. Due to the significance of their neurological functions, the normal spinal cord tissues were not collected. An *ex vivo* study can preliminarily validate the effectiveness of autofluorescence spectroscopy for tumor classification. In order to realize the distinction of spinal cord tumor tissues and normal tissues for intraoperative tumor boundary division, new detecting device will be developed for *in vivo* autofluorescence spectral measurement of the spinal cord. Furthermore, due to the limited data size, other statistical methods such as PCA or SVM could not be applied in this study. In the future, we plan to enlarge the data size to realize better classification results.

5. Conclusion

In conclusion, we developed an autofluorescence spectral measurement system and acquired the spectral properties of different types of spinal cord tumors *ex vivo* by it. Our results show

Biomedical Optics EXPRESS

that extramedullary tumors with negative GFAP possess significantly different autofluorescence spectral properties from intramedullary tumors with positive GFAP. The autofluorescence spectroscopy analysis method in our research is believed to act as an additional diagnostic tool for the intraoperative validation of tumor types and thereby help further surgical treatment in consideration of its real-time performance and result accuracy.

Funding

National Key Research and Development Program of China (2017YFC0108000, 2017YFC0108001), National Natural Science Foundation of China (81427803, 81771940), Beijing Municipal Natural Science Foundation (7172122, L172003), Beijing Municipal Science & Technology Commission (Z151100003915079).

Acknowledgments

The authors thank the Department of Neurosurgery and the Department of Pathology at Beijing Tsinghua Changgung Hospital for the provision of spinal cord tumor specimens and corresponding pathological reports.

Disclosures

The author declares that there is no conflict of interests regarding the publication of this article.